Fermi National Accelerator Laboratory

FERMILAB-Pub-76/48-EXP
7100.211

(Submitted to Nucl. Instrum. Methods)

# MEASUREMENTS AND CALCULATIONS OF CASCADES PRODUCED BY 300-GeV PROTONS INCIDENT ON A TARGET INSIDE A MAGNET

M. Awschalom, S. Baker, C. Moore, and A. Van Ginneken
Fermi National Accelerator Laboratory, Batavia, Illinois 60510

and

K. Goebel and J. Ranft
CERN, Geneva, Switzerland

May 1976

Operated by Universities Research Association Inc. under contract with the Energy Research and Development Administration

# MEASUREMENTS AND CALCULATIONS OF CASCADES PRODUCED BY 300-GeV PROTONS INCIDENT ON A TARGET INSIDE A MAGNET

M. Awschalom, S. Baker, C. Moore, and A. Van Ginneken
Fermi National Accelerator Laboratory, Batavia, Illinois 60510

and

K. Goebel and J. Ranft
CERN, Geneva, Switzerland

## ABSTRACT

A thick aluminum block placed between the pole pieces of a magnet was irradiated with 300-GeV protons. Responses of activation foils and dosimeters placed around the magnet and inside the gap were measured to study the propagation of high-energy cascades. Predictions of two different Monte Carlo calculations agree well with these measurements.

# I. INTRODUCTION

Shielding around the high-energy accelerators and experimental areas of Fermilab and at CERN has been designed with the help of Monte Carlo (MC) calculations[1-5] which simulate the development of hadronic cascades in bulk matter. These calculations, while sharing a large amount of common information, differ in their prescription of particle production in the interactions of hadrons with nuclei as well as in computational techniques. While comparisons of calculations with experiments for 30-GeV protons incident on a beam dump[5,6] are satisfactory, it is still necessary to make verifications at higher energies. A recent experiment[7] measured the temperature rise when 300-GeV protons were incident on targets of various materials. Calculations agree quite well with the results. However, because of the slender dimensions of the targets it reveals very little about the radial development of the cascade. The present experiment takes the comparison a significant step further in this direction.

A beam of 300-GeV protons was incident on a thick aluminum block placed between the pole pieces of a standard bending magnet. Sets of dosimeters and activation foils were placed at various locations outside and inside the magnet. The responses of these detectors are compared with those predicted by calculations. There is generally quite satisfactory agreement between measurements and calculations.

# II. EXPERIMENTAL

A 300-cm long Fermilab external beam bending magnet was installed in the pretarget hall of the Fermilab Neutrino Facility. An aluminum target

block 20.3-cm long and 3.2 × 8.3 $cm^2$ in cross section was placed 20 cm downstream from the upstream face of the magnet. The target blocked almost the entire aperture of the vacuum chamber of the magnet. The detectors were placed at regular intervals along each of four lines parallel to the magnet axis. Figure 1 is a simplified diagram of the geometry. The lateral positions of the four lines are indicated. The location of the detectors along the beam directions may be read off the graphs showing the results.

The activation foils used were aluminum (for measurement of $^{18}F$ and $^{24}Na$), copper ($^{24}Na$, $^{52}Mn$), polyethylene ($^{11}C$), and teflon ($^{18}F$). Dose delivered during the irradiation was measured using hydrogen pressure dosimeters,[8] radiophotoluminescent glass dosimeters,[9] and thermoluminescent dosimeters (TLD's) in the form of $^{6}LiF$ and $^{7}LiF$ pairs. The detectors placed inside the magnet (positions VC and B in Fig. 1) were mounted on wooden slats. This is illustrated in detail in Fig. 2.

A packet of beam monitor foils was placed 120 cm upstream of the target. One of each of the detector foils was present, separated by thin polyethylene foils. The entire packet was about 0.55 $g/cm^{-2}$ thick. The purpose of these foils was to facilitate data analysis. Calculations indicate that beam interactions in the monitor foils contributed significantly to the activation in foils located close to the upstream end of the magnet. From the assumed production cross section of $^{24}Na$ in copper (4.0 mb)[10] it was estimated that a total of $4.5 \times 10^{14}$ protons were incident on the monitor packet. The beam intensity varied considerably during the run, as witnessed by the variation in current of an air filled ionization chamber which was located in a nearby access labyrinth during the irradiation (see Fig. 3).

An estimate of the position and spatial extent of the beam was provided by autoradiographs of the aluminum target block. This showed the beam to be off center by about 0.9 cm. The beam was seen to be roughly circular with a radius of 0.4 cm. A rough idea of the extent and magnitude of beam halo was obtained by measuring activation of foil packets of Al ($^{24}$Na) and teflon ($^{18}$F) located at radial distances of 7.5 cm and 12.2 cm (in each of two azimuthal directions) just upstream of the monitor foil packet. Assuming the same production cross section for the halo particles as for high-energy protons, the results correspond to about $3.6 \times 10^{10}$ protons cm$^{-2}$ and $2.3 \times 10^{10}$ protons cm$^{-2}$ at radii of 7.5 cm and 12.2 cm respectively, with close agreement between results in the two different azimuthal directions. Calculations indicate that the halo was the largest source of activation in the detector foils upstream of the aluminum block.

Radioactivities of the species sought for in the foils were assayed using a 3 × 3-in. NaI(Tl) crystal connected to a dual single channel analyzer and/or a large (10% efficiency) Ge (Li) detector connected to a 4K channel pulse height analyzer. The activities of the detector foils were compared directly with that of the same foil in the monitor foil packet. From the known or estimated activation cross section of the incident protons the results are then readily expressed in units of atoms produced by one incident proton per cm$^3$ of target foil. Decay corrections to the measurements were made using the program CLSQ.[11]

Exposure levels on contact due to remanent radioactivity of the magnet were measured with natural-LiF TLD's during a period from 60 to 115 minutes following the irradiation.

## III. RESULTS

Results of the experiment are shown in Figs. 4-8 (along with calculated results, discussed below). Beam-on dose responses are plotted as a function of distance along the beam for each of the four lateral positions in Fig. 4 (and reproduced in Fig. 7). When presented in this fashion the familiar "transition curve" shape is apparent in each case. In line with past experience,[12] where two or more dosimeter responses are measured at a common location they agree within a factor of two.

Net remanent exposure rates are shown in Fig. 5 (and Fig. 8). As expected, they also resemble the familiar transition curves.

The results of the activation detector measurements are presented in Fig. 6. Again they may be broadly described as transition curves with detailed shapes depending upon location and type of reaction studied. The similarity in the production probability of $^{18}F$ from aluminum and $^{52}Mn$ from copper is perhaps worth pointing out. The fact that their ratio is, to very good approximation, the same everywhere is a consequence of the close similarity of their excitation functions. More accidentally, this ratio is very close to unity in the units adopted here.

## IV. CALCULATIONS

### A. CYLKAZ and MAGKA.

The MC codes used at CERN to evaluate radiation problems are based on empirical formulae to describe particle production in particle-nucleus collisions. These are in good agreement with experiments where checks have been made. The main uncertainty lies in the production of particles

with low momenta in the laboratory system.[2] Presently there are no reliable data or theoretical models available to describe this. Among the outputs of these calculations are star (nuclear interaction) densities and density of energy deposition (dose).

The present experimental data on integral dose during irradiation and on remanent exposure rate are compared with results from two different codes: CYLKAZ and MAGKA. Both these programs assume cylindrical symmetry.

In MAGKA the geometry is that of a hollow cylinder with a target placed on the cylinder axis. Both the target and the cylinder are assumed to be of iron. The target is 9-cm long and 2 or 0.75 cm in radius for the positions VC, B, U, and S respectively. These represent the target dimensions of the experiment scaled by the ratio of the interaction lengths of aluminum and iron. The doses at position VC (Fig. 1) were calculated from the energy deposition recorded in a radial region between 8 and 8.5 cm during a MC run for a hollow cylinder with inner radius ($r_1$) of 7 cm. Doses at B and U are estimated with $r_1$ = 14 cm in the radial regions 14-14.5 cm and 21-21.5 cm respectively. At position S the doses are evaluated with $r_1$ = 3 cm between 17 and 17.5 cm in the radial direction.

In the program CYLKAZ for the VC, B, and U positions the assumed geometry consisted of two concentric cylindrical shells of iron with inner and outer radii of 7-7.5 cm and 14-20 cm respectively, and an aluminum target of 4-cm radius present between 18 and 38 cm from the upstream face of the magnet. For the S position there is only one shell of iron with inner

and outer radii of 2-16 cm and an Al target of 1.5-cm radius. The doses at positions of VC, B, U, and S were evaluated in 0.5-cm wide radial bins beginning at r = 7, 14, 19.5, and 15.5 cm respectively. The CYLKAZ calculation, while in principle closer to the experimental geometry, proceeds much slower than MAGKA. Hence results are statistically less valid.

The density of energy deposition as measured by the various dosimeters as well as calculated by both programs are plotted as a function of depth at each of the four lateral locations in Fig. 4. CYLKAZ can be seen to underestimate the dose at small radii while MAGKA is in better agreement there. The differences may well be largely statistical in origin. In neither calculation was any correction applied for beam halo or interactions of the beam with the monitor foils. Their inclusion might well improve the fit.

The calculated star densities may be used to make predictions of remanent exposure rate. This assumes that the remanent exposure rate is proportional to the star density. The constant of proportionality is related to the length of irradiation (including variations of intensity with time), cooling time, and to the calculational model (in particular the low momentum cutoff).[13-15] For MAGKA with threshold set at 0.3 GeV it was assumed that:

$$\text{Exposure Rate} = 2.10^{-7} \times \text{Star Density} \times \text{Incident Flux}$$

for the exposure rate in units of (Roentgen $h^{-1}$), the star density expressed as (stars, $cm^{-3}$, $proton^{-1}$), and the incident flux as (protons $sec^{-1}$).

The comparisons are shown in Fig. 5. Where calculated results are statistically meaningful they are also in satisfactory agreement with experiment.

B. CASIM.

Fermilab's MC program, CASIM,[3] relies on the Hagedorn-Ranft particle production model[16] plus a semiempirical formula describing production of low-energy secondaries.[2] It makes extensive use of weighting and averaging techniques. CASIM may be adapted to arbitrary geometries and may be biased to optimize computer time usage.

To calculate the radioactivity induced in the foils a geometry close to the actual one was used. Dimensions and materials were essentially as in Fig. 1 except that the magnet coils were assumed to be solid iron. However, dosimeters, foils, mounting slats, and the vacuum chamber wall were either ignored or reflected slight adjustments of the other dimensions. All foils were assumed to be 20-cm long (in the beam direction), 2.5-cm wide and infinitesimally thin (in the radial direction). The incident particles were represented as a sum of three terms: (1) A 300-GeV proton beam of circular cross section (0.4-cm radius). The protons were uniformly distributed within it. The center line of the beam was assumed to be parallel to and displaced by 1 cm from the axis of the magnet in the direction of the location B (see Fig. 1). (2) A broad halo represented by a Gaussian spatial distribution fitted to the experimental data. The halo particles were assumed to travel parallel to the proton beam. Their type and momentum spectrum were assumed to be such as produced in the collision of a 300-GeV proton with an iron nucleus. (3) The particles resulting from collisions of the beam in the monitor foil packet. Particle types, angles, and momenta were taken from the distributions resulting from 300-GeV protons incident on aluminum.

Although only the totals are reported here, the results for each component were computed separately.

To estimate the amount of radionuclides of each species produced in the foils, excitation functions for the various reactions were stored in the computer for reference during the MC simulation. For incident protons, all of the reactions have been studied reasonably well over most of the energy range of interest (except perhaps above 30 GeV, where they were assumed to remain constant). The ones adopted in the present work were taken mostly from existing compilations.[17,18] For incident neutrons $^{11}C$ from carbon and $^{24}Na$ from aluminum are sufficiently well known experimentally.[17] For the production of $^{18}F$ from fluorine by neutrons the cross section is well known below 20 MeV;[19] above this it was assumed to be similar in shape to that of C(n, X) $^{11}C$. The remaining four excitation functions all involve deep spallation and were assumed to be identical to those for protons. For incident pions the excitation functions adopted did not distinguish between charge states. The only reaction reasonably well studied is $C(\pi^{\pm}, X)$ $^{11}C$.[18,20] For $F(\pi^{\pm}, X)$ $^{18}F$ the shape was assumed to be similar to the $C(\pi^{\pm}, X)$ $^{11}C$ reaction but normalized to a few measured values.[21] For all other nuclides the assumption was made that the production cross section was equal to that for protons with a kinetic energy equal to the pion's total energy. This is known to hold reasonably well for a number of spallation products from copper by 65 MeV $\pi^+$ and $\pi^-$, including $^{52}Mn$.[22] For reference, the basic excitation functions are shown in Fig. 9 in the same abbreviated form as they were stored in the computer. All others were derived from these in the prescribed manner.

The results of the calculation for the activation detectors are shown in Fig. 6. Considering the large uncertainties in assumed beam characteristics and excitation functions the results are quite satisfactory. The reaction $Al(n, \alpha)^{24}Na$ which has a large cross section at rather low energy (~10 MeV) seems to yield the poorest fits, especially at large lateral distances. This is not surprising since the calculational model cannot be expected to hold well at such low energies. Rather large discrepancies persist also in the region upstream of the target block. Here the problem rests likely with the crude model describing the off-beam incident particles.

The same calculation which predicts radionuclide production also computes the star density in iron for all hadrons above 0.3 GeV/c in momentum as a function of location. The conversion factor relating this star density to exposure rate was the same as the one used for the MAGKA results above. The comparisons are shown in Fig. 7. Again the calculation represents the results quite well.

A different calculation was performed to predict energy deposition. Centered at each of the four lateral positions a block of material having an infinitesimal density was introduced. Otherwise the geometry was the same as for the radionuclide production calculation. The low-density block, which does not perturb the cascade development, simulates a small detector. The block was divided into volumes measuring 20 cm along the beam direction and ranging in size from 3 $cm^2$ (VC) to 12 $cm^2$ (U) perpendicular to the beam direction, for the purpose of sampling the hadronic and electromagnetic showers. The error introduced by the larger extent of these detectors should

be tolerable in view of the other uncertainties. Figure 8 shows the comparisons which here also are quite satisfactory.

From the nature of the MC calculation, results in neighboring locations tend to be positively correlated. Caution must therefore be used in interpreting smoothness as lack of statistical error and also in trying to extrapolate results beyond the bounds of the calculation.

## V. CONCLUSIONS

At the highest accelerator energies presently available, both the CERN and Fermilab programs which are frequently called upon to evaluate shielding designs and study related problems, make predictions in good agreement with the present experiment. It should be emphasized that these comparisons are absolute, i. e., without any normalization between calculation and experiment.

While experimental checks over larger dimensions are awaited, the results of the present comparisons along with those of earlier ones should give confidence in the predictions of these programs when applied to different problems in this energy range.

## ACKNOWLEDGMENTS

We wish to thank Mr. J. Baldwin, Mrs. I. Klanner-Jarstorff, Dr. K. Lambert, and Mr. D. Voy for their help with the measurements. Thanks also to the Fermilab Accelerator Research Divisions for making this experiment possible.

## REFERENCES

[1] J. Ranft, Nucl. Instrum. Methods, 48, 133 (1967); , Particle Accelerators, 3, 77 (1971); , CYLKA, a Monte Carlo Hadron Cascade Calculation in Cylindrical Layers of Different Materials, CERN Lab II-RA/74-1 (1974).

[2] J. Ranft and J. T. Routti, FLUKA and MAGKA Monte Carlo Programs for Calculating Nucleon-Meson Cascades in Cylindrical Geometries, CERN Lab II-RA/73-2 (1973).

[3] A. Van Ginneken and M. Awschalom, High Energy Particle Interactions in Large Targets. Vol. I. Hadronic Cascades, Shielding and Energy Deposition, Fermilab, Batavia, Ill. (1975).

[4] A. Van Ginneken, CASIM, Program to Simulate Transport of Hadronic Cascades in Bulk Matter, Fermilab FN-272 (1975).

[5] T. W. Armstrong et al., Nucl. Sci. Eng., 49, 82 (1972).

[6] A. Van Ginneken, M. Awschalom and T. Borak, Comparison of Measurements and Calculation for a 29.4 GeV/c Steel Beam Stop, Int. Congress on the Protection against Accelerator and Space Radiation, p. 814, CERN 71-16 (1971).

[7] M. Awschalom et al., to be published in Nucl. Instrum. Methods.

[8] A. Morris, R. Sheldon and G. B. Stapleton, A Remote Reading Integrating Radiation Dosimeter for the Range $10^4$-$10^9$ Rad, RHEL/R-132 (1966).

[9] Toshiba FD-RI-I RPL glass dosimeters.

[10] S. Baker, Beam Intensity Measurements Using Copper Foils, Fermilab FN-276 (1975).

[11] J. B. Cumming, CLSQ. The Brookhaven Decay Curve Analysis Program, Proc. Symp. of Applications of Computers to Nuclear and Radiochemistry, NAS-NS-3107, p. 25 (1962).

[12] J. T. Routti and M. Van de Voorde, Intercomparison of High-Dose Dosimeters in Accelerator Radiation Fields, Nucl. Instrum. Methods, 99, 563 (1972).

[13] K. Goebel, J. Ranft, and G. R. Stevenson, Chap. VIII of Radiation Problems Encountered in the Design of Multi-GeV Research Facilities, K. Goebel Ed., p. 101, CERN Lab. II/71-21 (1971).

[14] T. W. Armstrong and R. G. Alsmiller, Jr., Calculation of the Residual Photon Dose Rate around High-Energy Proton Accelerators, ORNL-TM-2498 (1969).

[15] A. H. Sullivan and R. H. Overton, Health Phys., 11, 1101 (1965).

[16] R. Hagedorn, Suppl. Nuovo Cimento, 3, 147 (1965); R. Hagedorn and J. Ranft, Suppl. Nuovo Cimento, 6, 169 (1968); H. Grote, R. Hagedorn and J. Ranft, "Atlas of Particle Spectra", CERN, Geneva (1970).

[17] St. Charalambus, J. Dutrannois, and K. Goebel, Particle Flux Measurements with Activation Detectors, CERN/DI/HP 90 (1966).

[18] R. Silberberg and C. H. Tsao, Cross Sections of Proton-Nucleus Interactions at High Energies, NRL Report 7593 (1973).

[19] M. Bormann, H. Neuert, and W. Scobel, Tables and Graphs for (n, p), (n, $\alpha$), and (n, 2n) Reactions in the Neutron Energy Region 1-37 MeV, Handbook on Nuclear Activation Cross Sections, p. 87, IAEA, Vienna (1974).

[20]B. J. Dropesky, Phys. Rev. Lett., 34, 821 (1975).

[21]P. J. Karol, Phys. Lett., 58B, 489 (1975).

[22]C. K. Garrett and A. L. Turkevich, Phys. Rev., C8, 594 (1973).

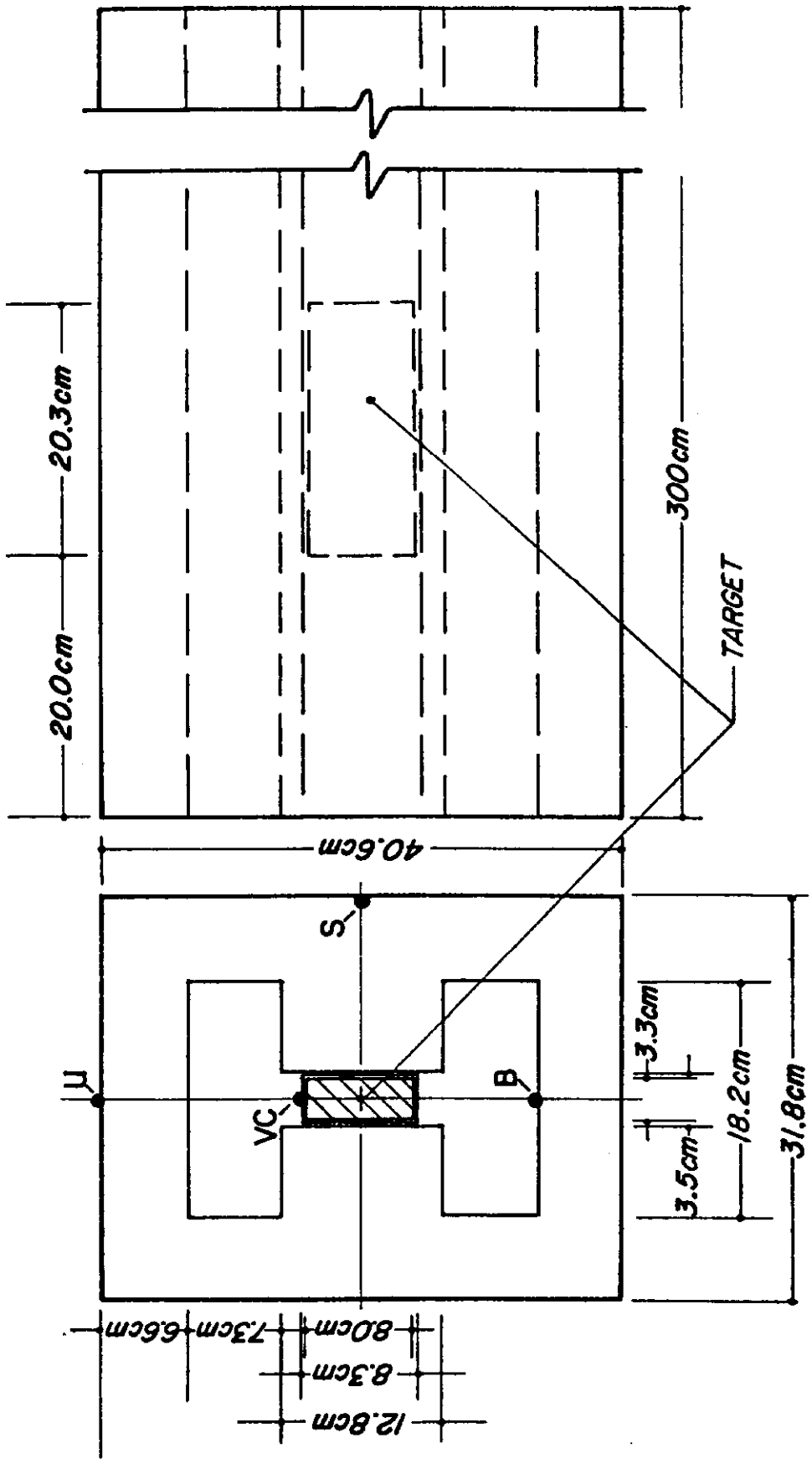


Fig. 1. Simplified drawing of experimental setup. At the lateral positions VC, B, U, and S detectors were placed parallel to the center line of the magnet.

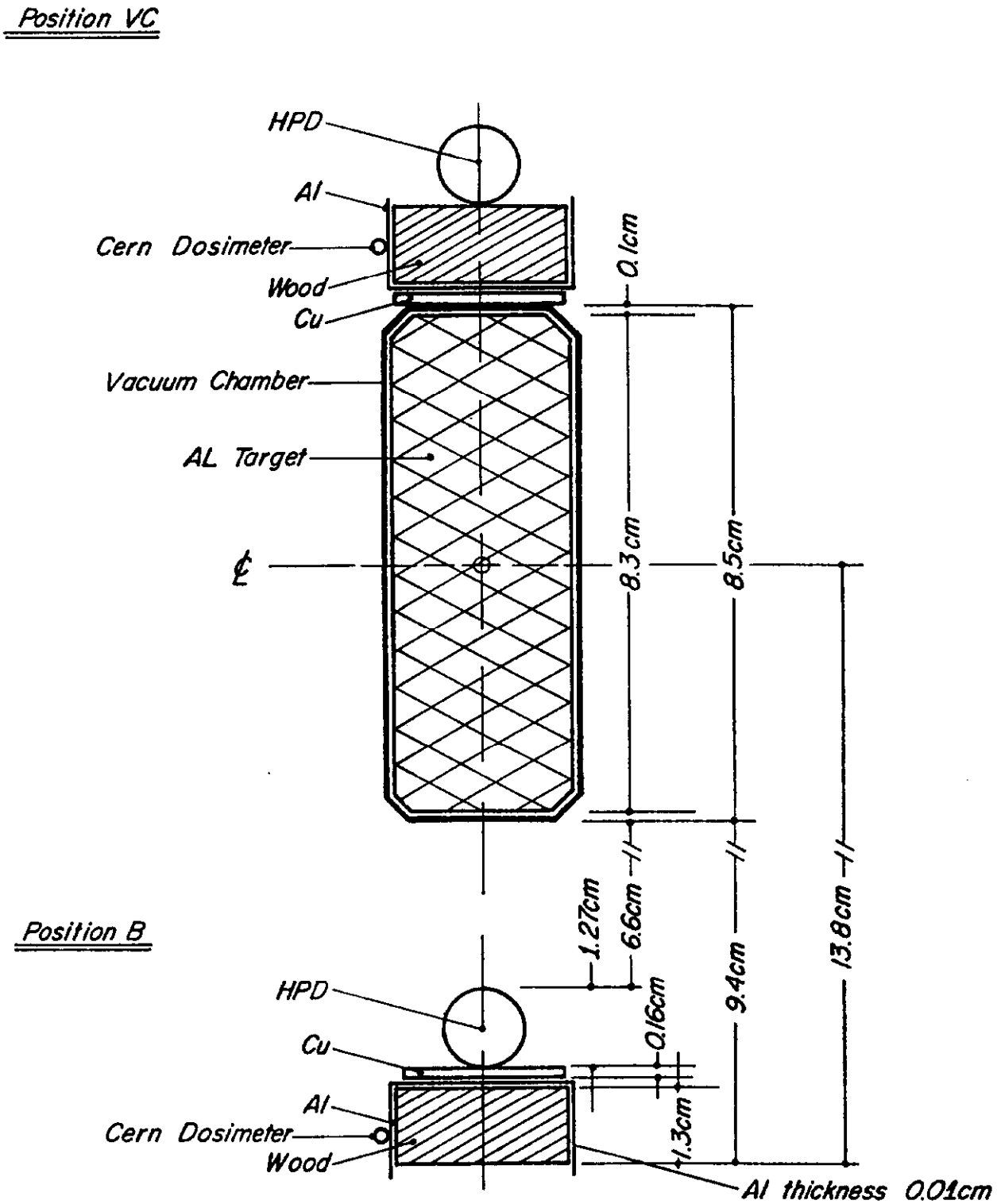


Fig. 2. Detailed cross section of positioning of activation foils and dosimeters for locations VC and B of Fig. 1.

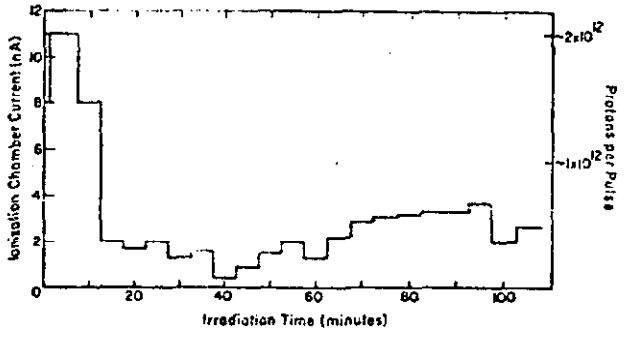


Fig. 3. Current measured during irradiation by an air filled ionization chamber located in an access labyrinth near the magnet.

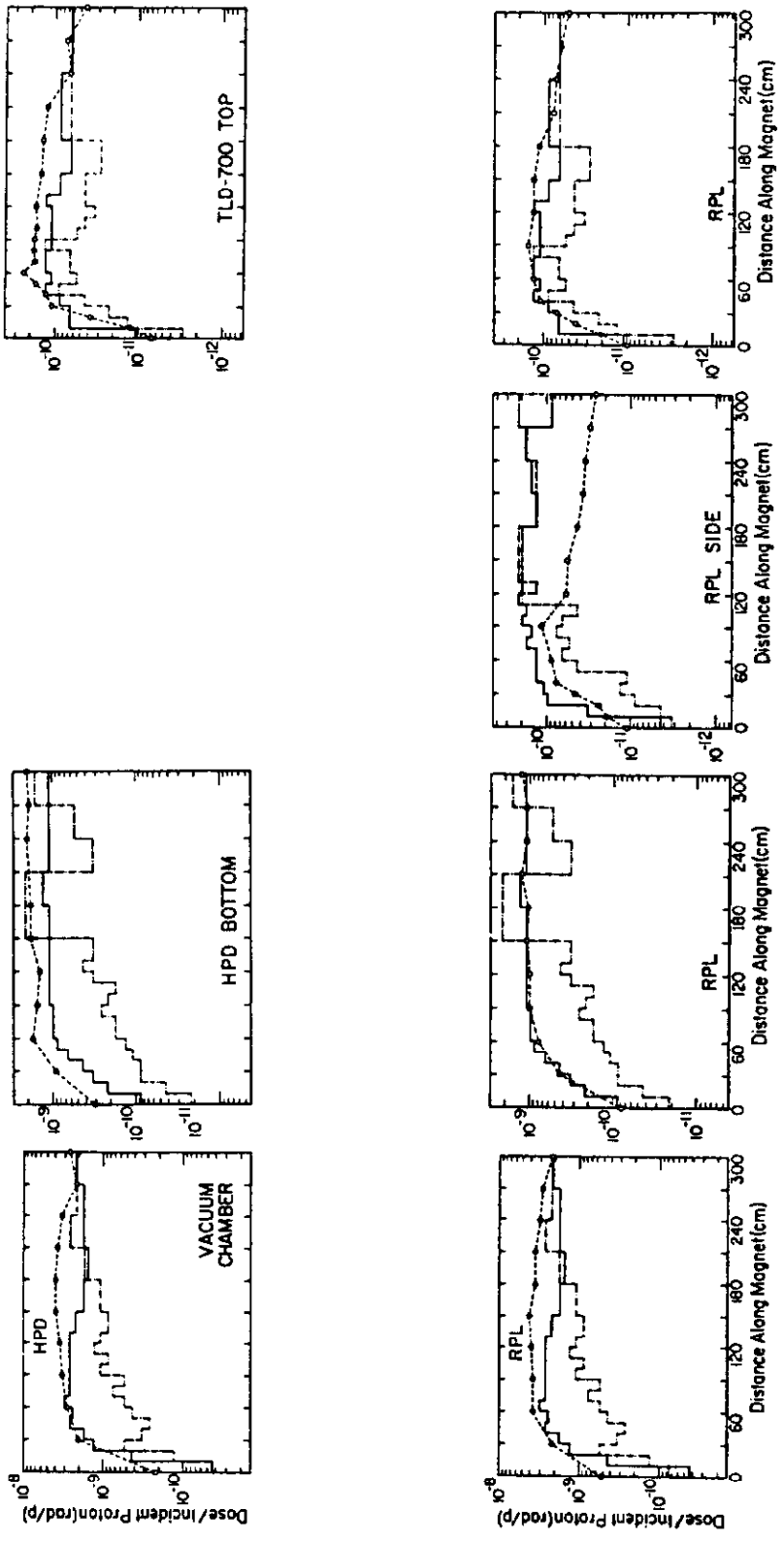


Fig. 4. Measured doses incurred during irradiation for each of the four lateral positions (---o---) along with predictions of CERN calculations MAGKA (———) and CYLKAZ (———).

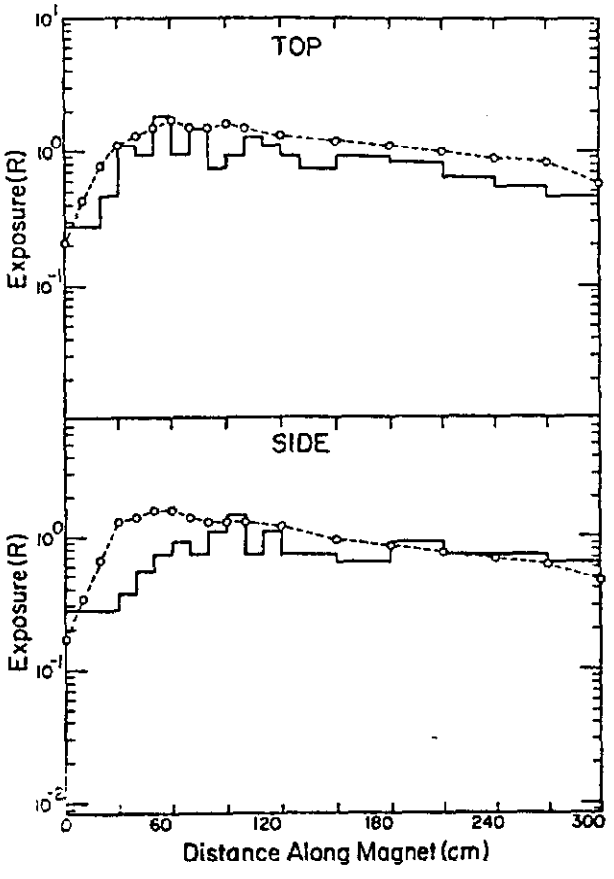


Fig. 5. Measured exposures following irradiation for cooling time of 60 minutes and integration time of 55 minutes at positions U and S (---o---) along with predictions of CERN calculation MAGKA (———).

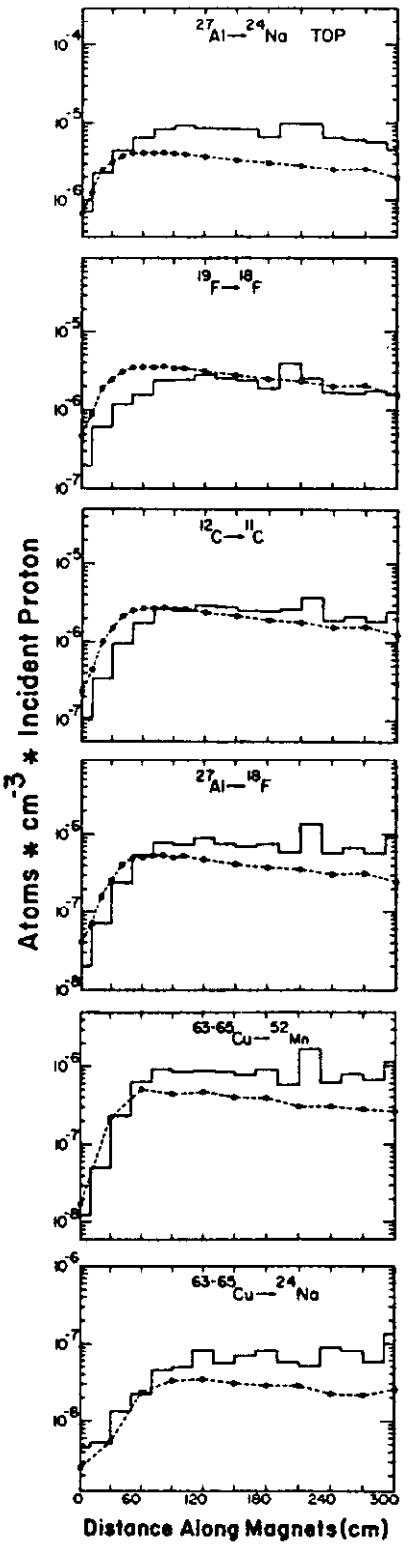


Fig. 6a

Fig. 6. Induced radioactivity measured in various foils at each of the four lateral positions (---o---) along with predictions of Fermilab calculation CASIM (———).

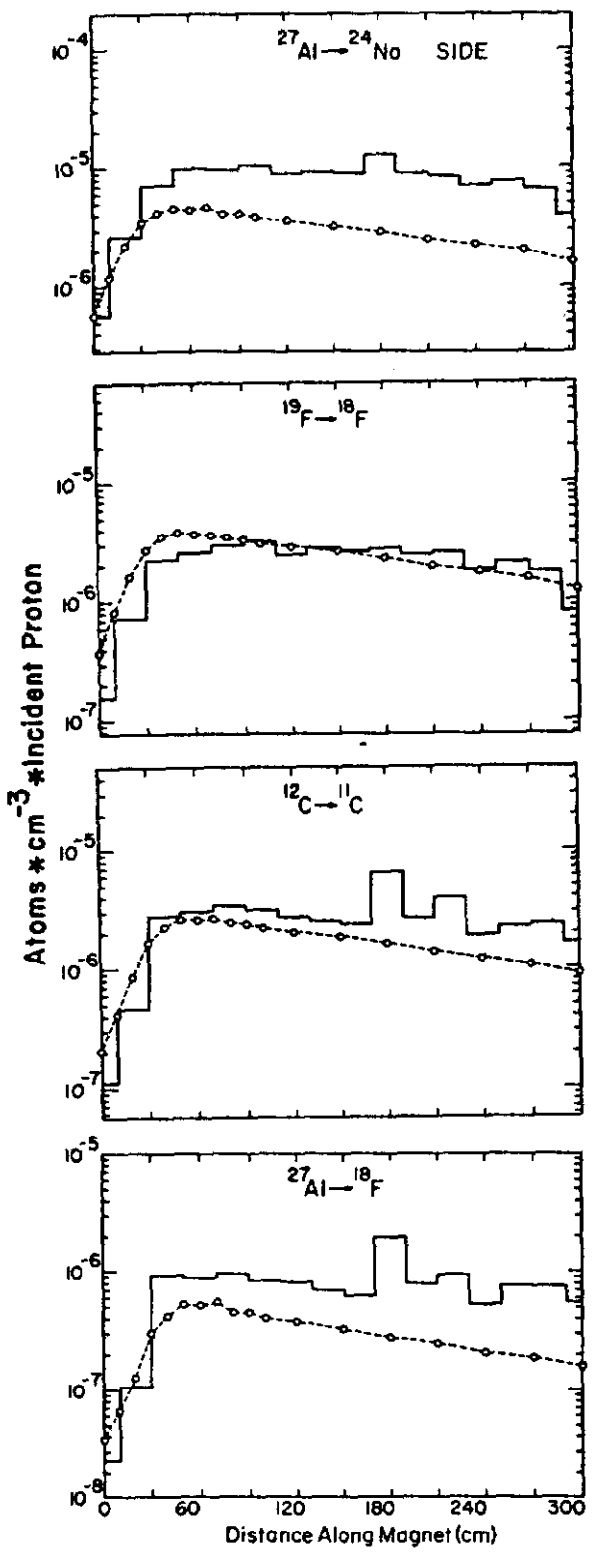
$^{27}Al \rightarrow ^{24}Na$ SIDE
$^{19}F \rightarrow ^{18}F$
$^{12}C \rightarrow ^{11}C$
$^{27}Al \rightarrow ^{18}F$
Atoms * cm$^{-3}$ * Incident Proton
Distance Along Magnet (cm)
0
60
120
180
240
300

Fig. 6b

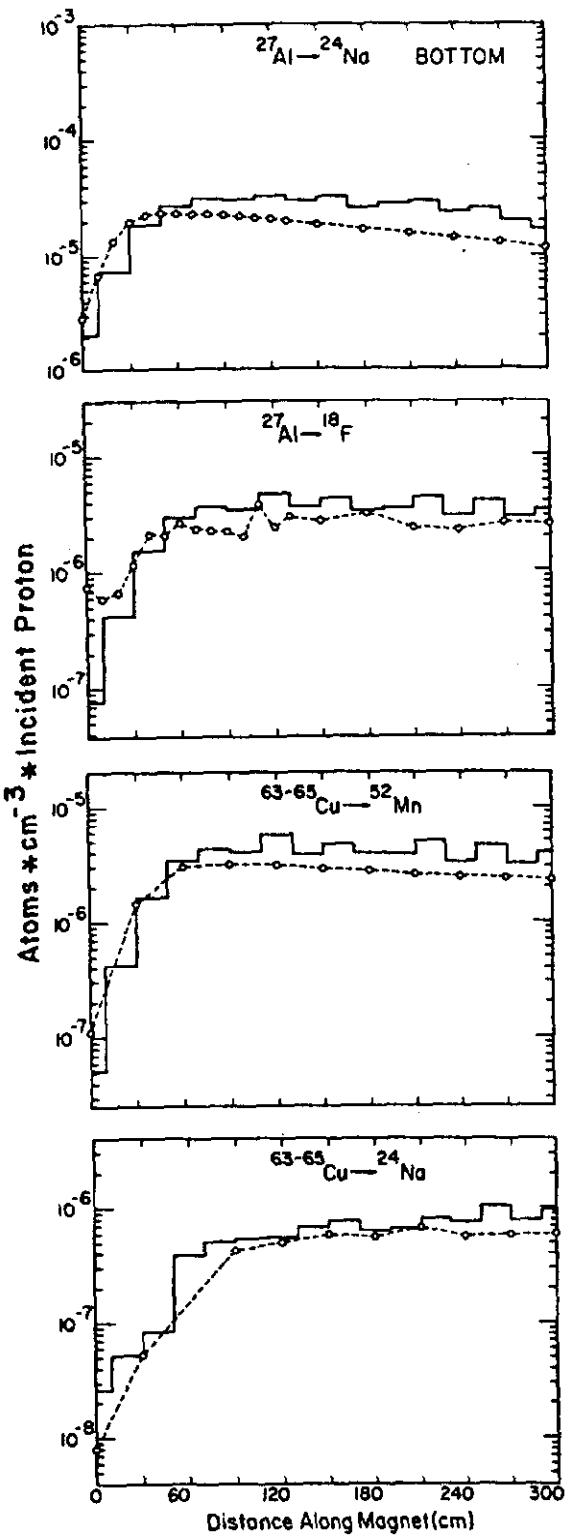
$^{27}Al \rightarrow ^{24}Na$ BOTTOM
$^{27}Al \rightarrow ^{18}F$
$^{63-65}Cu \rightarrow ^{52}Mn$
$^{63-65}Cu \rightarrow ^{24}Na$
Atoms * cm$^{-3}$ * Incident Proton
Distance Along Magnet (cm)
0
60
120
180
240
300

Fig. 6c

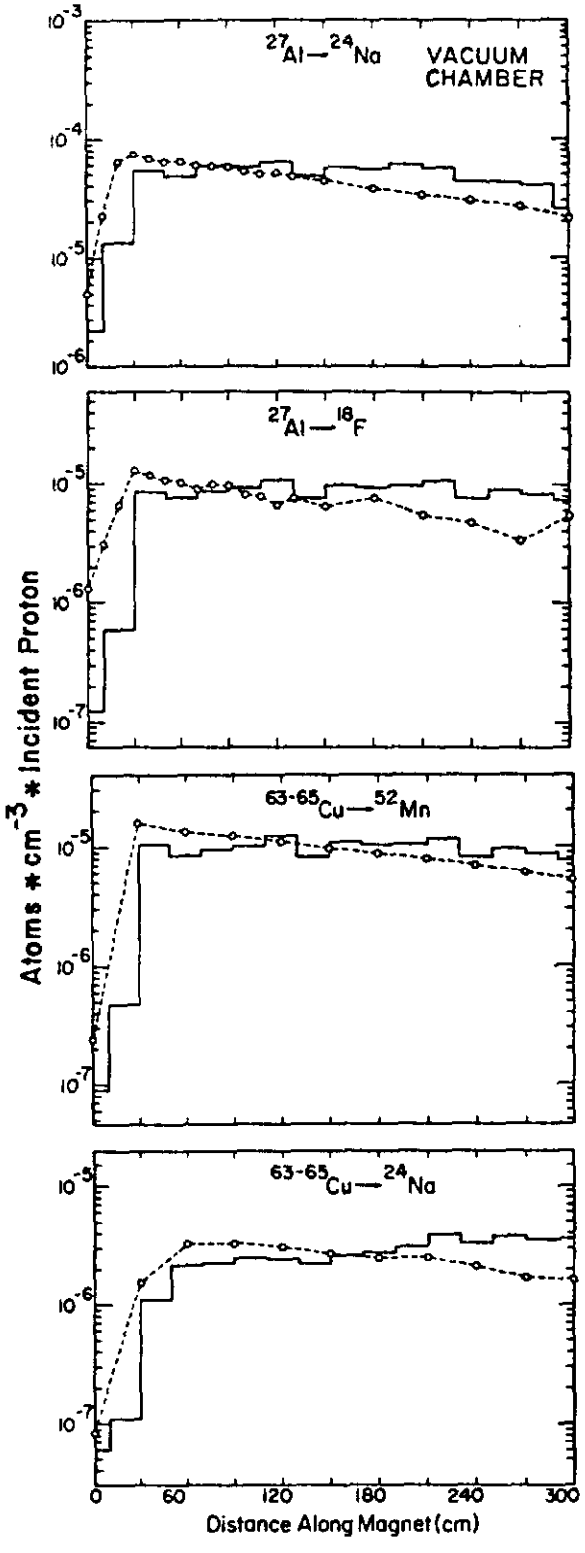
$^{27}Al \rightarrow ^{24}Na$ VACUUM CHAMBER
$^{27}Al \rightarrow ^{18}F$
$^{63-65}Cu \rightarrow ^{52}Mn$
$^{63-65}Cu \rightarrow ^{24}Na$
Atoms * cm$^{-3}$ * Incident Proton
Distance Along Magnet (cm)
0
60
120
180
240
300

Fig. 6d

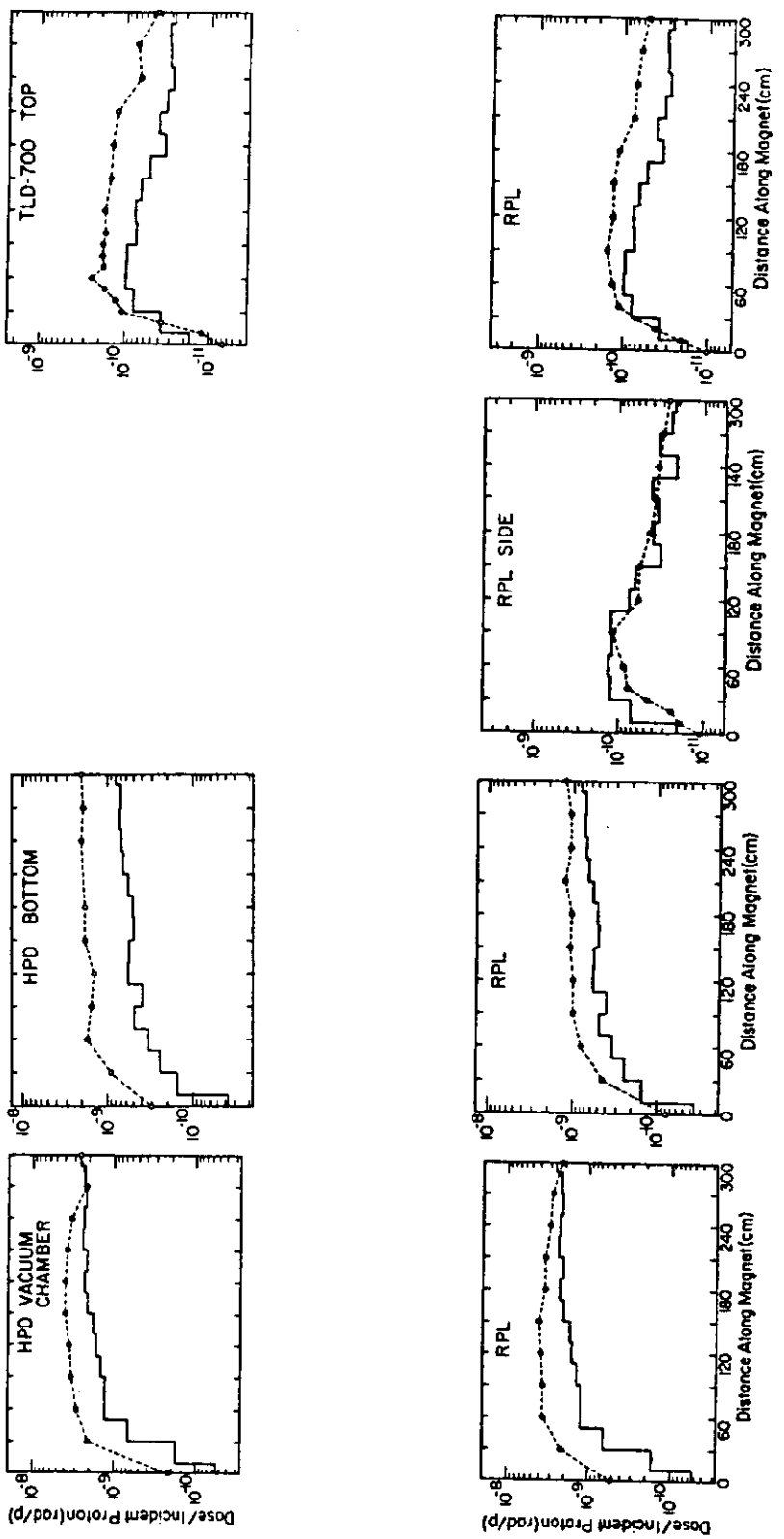


Fig. 7. Measured doses incurred during irradiation for each of the four lateral positions (---o---) along with predictions of Fermilab calculation CASIM (———).

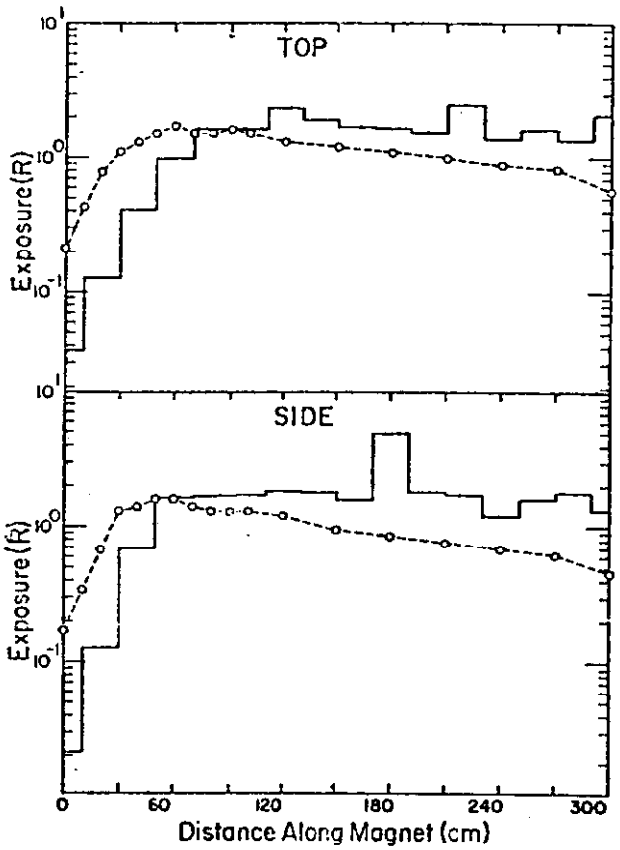


Fig. 8. Measured exposures following irradiation for cooling time of 60 minutes and integration time of 55 minutes of positions U and S (---o---) along with predictions of Fermilab calculation CASIM (———).

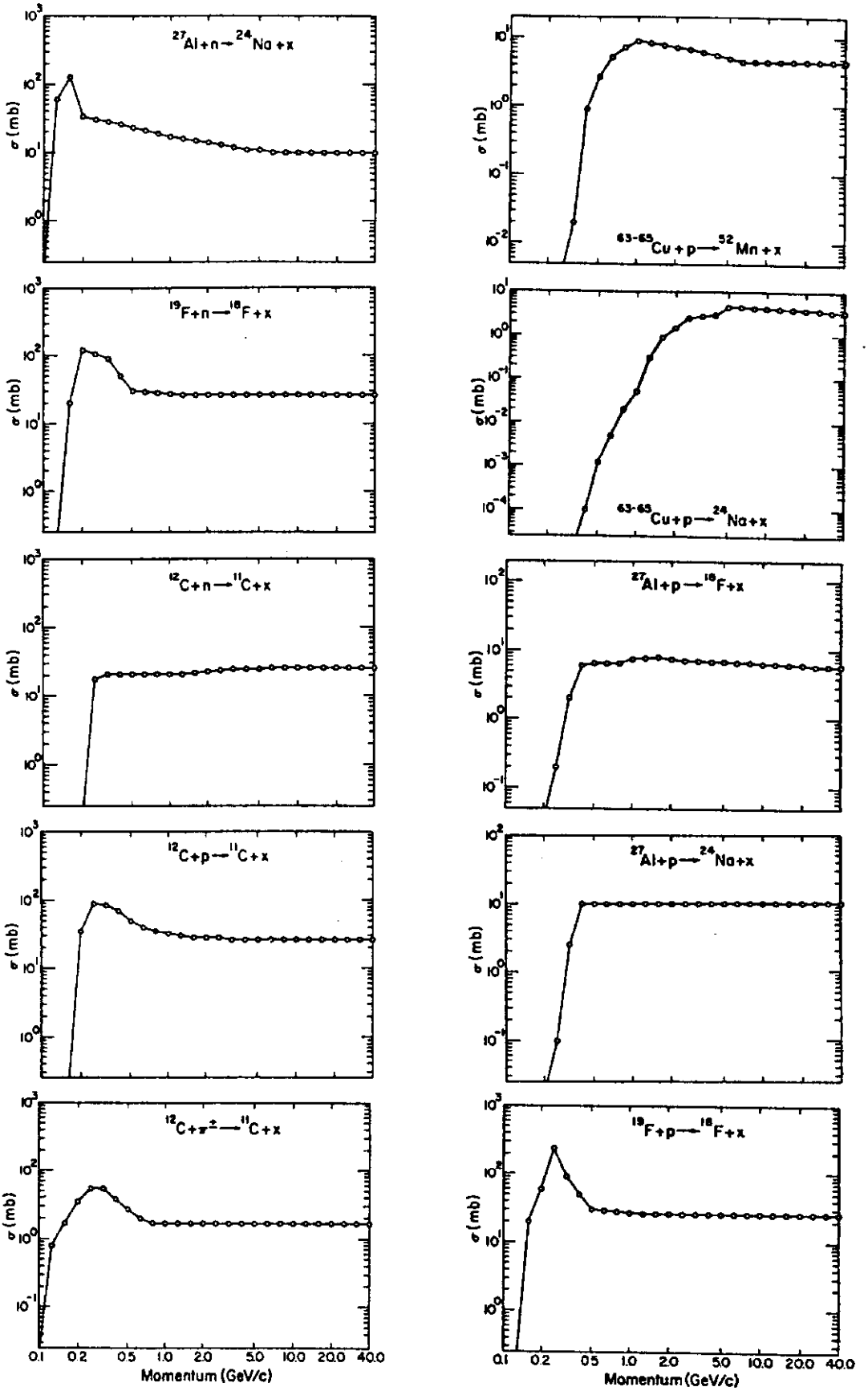


Fig. 9. Experimental excitation functions used in program CASIM to predict induced radioactivities in the foils. Other needed excitation functions were derived in simple fashion from those shown here.